

Strain demand prediction method for buried X80 steel pipelines crossing oblique-reverse faults

Xiaoben Liu^{*1}, Hong Zhang¹, Xiaoting Gu^{**2}, Yanfei Chen¹, Mengying Xia¹ and Kai Wu¹

¹College of Mechanical and Transportation Engineering, China University of Petroleum-Beijing, Beijing, China

²College of Petroleum Engineering, Yangtze University, Wuhan Hubei, China

(Received December 27, 2016, Revised February 26, 2017, Accepted March 10, 2017)

Abstract. The reverse fault is a dangerous geological hazard faced by buried steel pipelines. Permanent ground deformation along the fault trace will induce large compressive strain leading to buckling failure of the pipe. A hybrid pipe-shell element based numerical model programed by INP code supported by ABAQUS solver was proposed in this study to explore the strain performance of buried X80 steel pipeline under reverse fault displacement. Accuracy of the numerical model was validated by previous full scale experimental results. Based on this model, parametric analysis was conducted to study the effects of four main kinds of parameters, e.g., pipe parameters, fault parameters, load parameter and soil property parameters, on the strain demand. Based on 2340 peak strain results of various combinations of design parameters, a semi-empirical model for strain demand prediction of X80 pipeline at reverse fault crossings was proposed. In general, reverse faults encountered by pipelines are involved in 3D oblique reverse faults, which can be considered as a combination of reverse fault and strike-slip fault. So a compressive strain demand estimation procedure for X80 pipeline crossing oblique-reverse faults was proposed by combining the presented semi-empirical model and the previous one for compression strike-slip fault (Liu 2016). Accuracy and efficiency of this proposed method was validated by fifteen design cases faced by the Second West to East Gas pipeline. The proposed method can be directly applied to the strain based design of X80 steel pipeline crossing oblique-reverse faults, with much higher efficiency than common numerical models.

Keywords: oblique-reverse fault; strain demand; hybrid finite element model; parametric analysis; regression equation

1. Introduction

In the last few years, the demand of natural gas in China has been increased rapidly, a great number of high strength pipelines have been constructed in China, which are generally recognized as the safest and most economical method for transporting natural gas over long distances (Lower 2014). The active fault is a main threat for these buried oil and gas pipelines (O'Rourke *et al.* 2012). Large ground movement along the fault trace will cause large tensile or compressive strain in the pipe leading to potential failure of rupture or buckling, which is especially dangerous for high pipe pressure gas pipeline. Once the fire or explosion induced by gas leakage happens, it may result in serious accidents with loss of money and even human life. Pipelines could be subjected to different types of faulting such as normal, reverse, strike-slip or a combination of these faults, referred to as oblique reverse and oblique normal faulting, as shown in Fig. 1 (Rofooei *et al.* 2015).

Intensive research has been carried out for the mechanical performance of buried pipelines under fault displacements. Pertinent pioneer work was conducted by

Newmark and Hall (1975), who developed a simplified analytical model for predicting axial tensile strain. Thereafter, a large amount of analytical methods for strain analysis of pipeline under fault displacement have been proposed by Kennedy *et al.* (1977), Wang *et al.* (1985), Karamitros *et al.* (2007, 2016) and Trifonov *et al.* (2010 2012). But their methods are not available for pipelines under compression, such as in the cases of reverse faults.

For pipelines under compression, numerical analysis using the finite element method is the main chose, for its ability in highly nonlinear mechanical problems. A great number of researches are available on the numerical analysis of buried pipeline under fault movements. The beam-type FE model is suggested to be implemented by ALA 2001, Eurocode 8 - Part 4 and other pertinent structural codes. Melissianos *et al.* (2016), Joshi *et al.* (2011), Uckan *et al.* (2015) employed this model in numerical simulation of pipeline performance at fault

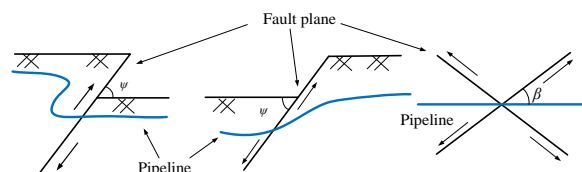


Fig. 1 Pipeline deformations under different active fault: (a) reverse fault (cross-section) (b) normal fault (cross-section) (c) strike-slip fault (plan view)

*Corresponding author, Ph.D.

E-mail: xiaotingu@aliyun.com

**Co-Corresponding author, Ph.D. Candidate

E-mail: liuxiaoben1991@126.com

crossings. Takada *et al.* (2001), Karamitros *et al.* (2007), and M. Liu *et al.* (2008) proposed a beam-shell hybrid model. A. Liu *et al.* (2004) proposed an equal boundary shell model. Gu *et al.* (2009) and Liu *et al.* (2016) developed a simple pipe-elbow hybrid model. Xie (2008) compared numerical model results with experimental results derived by Da Ha (2007) and validated the accuracy of the numerical results. Some rigorous numerical tools have also been used in recent years for analyzing the mechanical behavior of pipeline under fault movements (Vazouras *et al.* 2010, 2012, 2015, Trifonov *et al.* 2014, Zhang *et al.* 2014). In these models, continue solid elements were adopted to simulate the soil, and contact and friction conditions were considered on the soil-pipe interface. Notable full scale experimental work on the strain and stress reaction of buried pipelines due to reverse fault has been done by Rafooei *et al.* (2015) and Jalali *et al.* (2016), which provides precious experimental results for validating numerical models.

However, numerical methods also have some limitations for engineering application. They need experienced experts and are time consuming if the number of calculation is large. So regression-based relationships can be used to provide simple and efficient functions for these ground movement induced pipe strains as suggested by CSA Z662 (2011). Shokouhi *et al.* (2013) and Saberi *et al.* (2013) obtained the relationships for some special cases of buried high density polyethylene (HDPE) pipelines and X65 pipeline respectively. For X80 steel pipelines, Liu *et al.* (2016) proposed a semi-empirical model for strain demand prediction for X80 pipeline at compression strike-slip fault crossings with the consideration of soil parameters. This method has effectively simplified the strain calculation procedure, however, it is also limited in predicting the pipe behavior in horizontal plane. So the strain behavior of pipeline in vertical plane also need to be investigated, for the oblique reverse faults are commonly encountered in engineering practice. Fig. 2 illustrates the pipeline response subjected to reverse fault, when pipe-fault crossing is perpendicular ($\beta=90^\circ$). It is under compression combined with bending in the vertical plane.

In this study, a systematic investigation was carried out first to provide a simple and accurate strain prediction

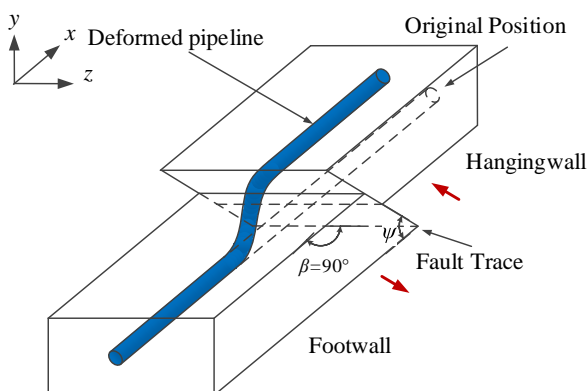


Fig. 2 Schematic representation of buried pipeline subjected to reverse fault displacement when $\beta=90^\circ$

method for buried X80 steel pipelines under reverse faulting in the vertical plane. A hybrid pipe-shell element numerical model was developed to study the strain behavior of the pipe, accounting for large strain behavior of the pipeline. Accuracy of the model was validated by comparing the numerical results with full scale experimental results (Jalali *et al.* 2016). Influences of the pipe diameter, pipe wall thickness, fault displacement, fault dip angle, internal pressure and soil properties on the strain demand were studied in detail. A regression-based empirical equation for strain demand prediction was also proposed. Accuracy of the model was validated by comparing the predicted results with numerical results of 15 true design cases of the Second West to East gas pipeline in China. With the combined utilization of this proposed semi-empirical model and the previous one for compression strike-slip fault (Liu *et al.* 2016), it is possible to obtain the strain demand of X80 pipeline under common faced oblique reverse faults in engineering practice with much less effort and time consumption compared to nonlinear finite element models.

2. Strain based design method for steel pipelines under soil movements

Strain based design method (SBD) is widely used in recent decades for the design of steel pipeline subjected to geological hazard induced permanent ground deformation (O'Rourke *et al.* 2012, Liu *et al.* 2009, Mohr 2003). Because ground movement in geological hazard areas often leads to axial plastic strain in the pipe, which indicates that the generalized stress based design method is inapplicable (Lower 2014). The purpose of SBD is to maintain pipeline integrity under large longitudinal plastic strains. SBD encompasses both strain demand (applied strain) ε and strain capacity (strain limit) ε_{crit} . The design object is to keep the strain demand of pipe less than the strain capacity with a safety factor f_s as shown in Eq. (1)

$$\varepsilon \leq f_s \varepsilon_{crit} \quad (1)$$

Two ultimate states are normally associated with SBD: tensile rupture and buckling. In case of reverse fault displacement, the pipe is mainly under compression. So, in this study, the peak axial compressive strain in the pipe and the critical buckling strain are the strain demand and strain capacity, respectively. And as mentioned in the Introduction part, for the complexity of pipe response in this situation, numerical models are the main tools to derive the strain demand. While, for strain capacity, series of method were available for API standard line-pipe steels. According to Q/SY GJX 0136, 2008, the adopted one in the design of the Second West to East Gas Pipeline, is proposed by CSA Z662.

3. Numerical model for pipeline crossing reverse fault

3.1 Pipe-soil interaction model

The motion of buried pipeline under faulting is constrained by the surrounding soil. The pipe-soil interaction can be simulated using two kinds of methods. One is through nonlinear soil springs in the axial, lateral, and vertical directions of the pipe, which are widely used in engineering design (Karamitros *et al.* 2007, Trifonv *et al.* 2010, Liu *et al.* 2004, Liu *et al.* 2008, Gu *et al.* 2009, Liu *et al.* 2015, 2016, Xie 2008, Shokouhi *et al.* 2013, Saberi *et al.* 2013). Soil springs in combination with pipe meshing with shell elements may lead to the introduction of local forces on shell elements that, especially in case of coarse mesh, do not represent well the physical problem, as they alter the distribution of stresses and strains on the pipeline wall, hence local buckling considerations are inaccurate. The other one is the contact and friction on the pipe-soil interface (Xie 2008, Vazouras *et al.* 2010, 2012, 2015, Gantes *et al.* 2013, Trifonv *et al.* 2014, Zhang *et al.* 2014). The first method was adopted for its simplicity and accuracy for compressive strain calculation. The soil springs are illustrated in Fig. 3. The elastic-plastic relationships for the peak forces and yield displacements of soil springs can be defined by two parameters, i.e., the peak force per unit length in the axial, lateral, vertical uplift and bearing directions, as illustrated in Fig. 4. T_u , P_u , Q_u and Q_d represent the peak force per unit pipe length in the axial, lateral, vertical uplift and bearing directions, respectively. Δp , Δt , Δq_d and Δq_u represent the yield displacements in the axial, lateral, vertical uplift and bearing direction, respectively. The detailed calculation methods provided by ALA Guideline (2001) for these parameters can be found in Section 4.1. It should be mentioned that soil spring force-displacement relationship in the vertical direction is not symmetric as the axial and lateral ones. Because pipe upward movement results to vertical forces at the pipe-soil interface whose maximum correspond to the weight of an inverted triangle prism of soil above the top of the pipe, and pipe downward movement results to vertical forces at the pipe-soil interface, which correspond to the vertical bearing capacity of a footing (O'Rourke and Liu 2012).

3.2 Pipe material model

The high strength X80 steel was adopted here as in the previous study for investigating the pipe strain in strike-slip fault conditions (Liu *et al.* 2016). The Ramberg-Osgood model (Ramberg and Osgood 1943) was used to describe

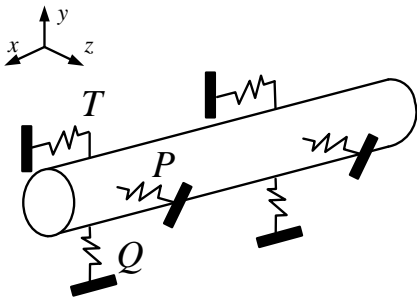


Fig. 3 Nonlinear soil spring model simulating soil constrain on pipe

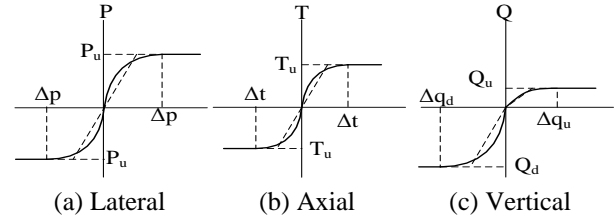


Fig. 4 Force-displacement relationships for nonlinear soil springs

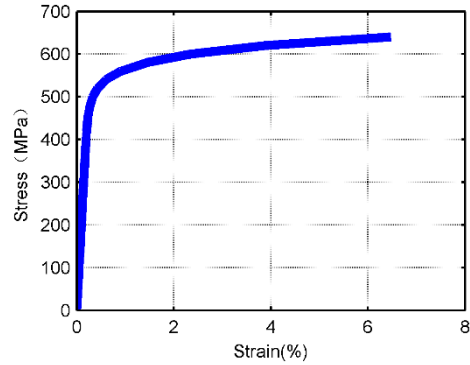


Fig. 5 True Stress-strain relationship for X80 pipe steel

the stress-strain relationship in Fig. 5. The formula of this model is

$$\varepsilon_{true} = \frac{\sigma}{E} \left[1 + \frac{n}{1+r} \left(\frac{\sigma_{true}}{\sigma_0} \right)^r \right] \quad (2)$$

Where E is the initial elastic modulus, $E=2.06 \times 10^5$ MPa; ε_{true} is the true strain; σ_{true} is the true stress, MPa; σ_0 is the yield stress of the pipe steel, $\sigma_0=530$ MPa; n and r are parameters of the Ramberg-Osgood model, $n=15.94$, $r=15.95$.

3.3 Finite element model

When a pipeline is crossing a reverse fault in vertical plane, the fault displacement applied on the pipeline can be calculated by two geometrical parameters, the fault displacement δ_v and the fault dip angle ψ , as shown in Fig. 6. The components of the fault displacement applied on the pipe can be calculated by Eq. (3)

$$\begin{aligned} \delta_x &= -\delta_v \cos \psi \\ \delta_y &= \delta_v \sin \psi \end{aligned} \quad (3)$$

Where δ_x is the fault displacement in the pipe axial direction, δ_y is the fault displacement in the pipe perpendicular direction.

A hybrid pipe-shell numerical model was adopted in this study, as it is more applicable for simulating local mechanical behavior than the elbow elements used in the previous study (Liu *et al.* 2016), and Zheng *et al.* (2016) showed that the computing time of the pipe-shell model is only a little larger than that of the elbow model. In this

model, the length of pipe was also set to be 1200 m, with 200-meter-long pipe near the fault trace modeled by S4R-type shell elements provided by ABAQUS. The shell elements are all 0.1m long in the axial direction of the pipe, which can accurately calculate the axial pipe strain, and 36 shell elements were used in the circumferential direction of the pipe. The other 1000-meter-long pipe in the two sides were all simulated by 1 m long PIPE31 elements. Distributing coupling constraint provided by ABAQUS was used in the interface of the two kinds of elements, as it can couple the displacement and rotation of the reference node to the average motion of the surface nodes (ABAQUS 2011). Zheng *et al.* (2016) also proved that the calculated pipe strain by this kind of coupling is almost the same with pure 1200 m-long-shell element model. SPRING2 elements developed by ABAQUS were used to constitute the nonlinear soil springs simulating the elastic-perfectly plastic force-displacement relationships of the pipe soil interaction model described in Section 3.1. Details of the presented model was illustrated in Fig. 6. Two load steps were needed in the analysis. The first is pressure load step, in which all the soil ends of soil springs were constrained, and internal pressure was applied to both shell and pipe elements. The second is fault movement step, in which all soil nodes in the footwall side remained constrained, while all soil nodes in the hangingwall side were applied with a displacement load simulating the fault movement. It should be also noticed that although in actual cases, the ground rupture is a dynamic process, while in most presented studies, the quasi-static condition was adopted for analysis (Joshi *et al.* 2011, Vazouras *et al.* 2010 2012 2015, Trifonov *et al.* 2014, Zhang *et al.* 2014 Jalali *et al.* 2016, Liu *et al.* 2008, Liu *et al.* 2016). So the loading rate of the soil movement was not considered neither in this study. Because numerous calculations are needed in the parametric analysis, the finite element model is programed in INP code supported by ABAQUS solver, which makes the batched calculation achievable.

3.4 Model validation by full scale experiment results

Jalali *et al.* (2016) conducted two series of full scale experiments on buried API Grade B steel pipeline under reverse fault displacement. One for pipes with diameter of 114.3 mm, another for pipes with diameters of 168.3 mm. The latter one was adopted here to check the accuracy of the finite element model. The soil parameters and steel

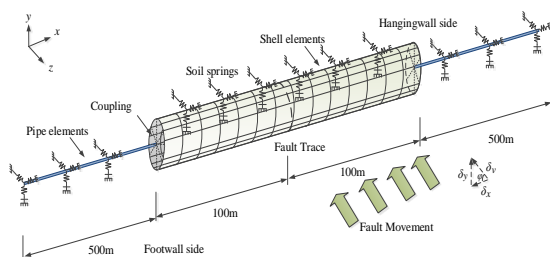
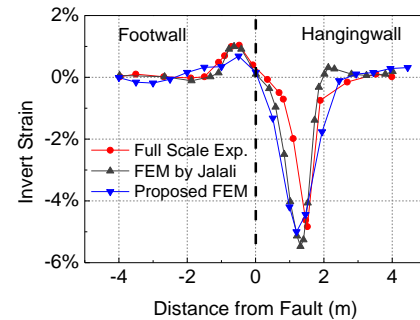


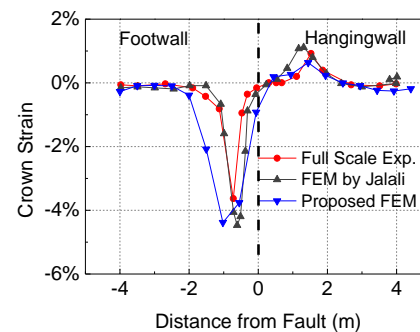
Fig. 6 Hybrid finite element model for buried pipeline subjected to reverse fault displacement

Table 1 Parameters of the experiment (adapted from Jalali *et al.* 2016)

Pipe diameter	Pipe wall thickness	Buried depth of pipe	Fault dip angle	Fault Displacement
$D(\text{mm})$	$t(\text{mm})$	$H(\text{m})$	$\psi(^{\circ})$	$\delta(\text{mm})$
168.3	4.4	1	61	600



(a) Invert strain



(b) Crown Strain

Fig. 7 Experimental and numerical invert and crown strain distribution along the pipe

parameters were all obtained from the experiment. Detailed parameters were listed in Table 1.

A same mesh rule with the FE model by Jalali *et al.* (2016) for the shell elements were adopted here to make the comparison results reasonable. Thus, the pipe length was redefined to be 8 m and the pipe was modeled by 6400 S4R elements with 16 shell elements around the pipe section. Fig. 7 illustrates the crown and invert strain distribution along the pipe axis. Results show that, the peak compressive invert strain appears in the hanging wall side, while the peak compressive strain appears in the Footwall side. And the peak invert strain is larger than the peak crown strain. This is induced by the asymmetry of vertical soil spring in the two directions. And comparing with the experimental and numerical results by Jalali *et al.* (2016), this proposed numerical model is accurate in strain calculation.

4. Results and discussion

4.1 Range of the parameters

Strain analysis of buried pipeline under fault displacement is a very complicated and challenging

problem. The mechanical response of pipe is highly nonlinear and the influence parameters are various. As Liu *et al.* (2016) concluded, four types of parameters must be considered:

Fault parameters: the fault displacement (δ_v) and the dip angle (ψ).

Pipe dimension parameters: the pipe diameter (D), and the wall thickness (t).

Load parameter: the internal pressure (p).

Soil property parameters: the internal friction angle of the soil (ϕ), the soil cohesion representative (c), the effective unit weight of soil (γ) and the reduction factor (f).

In this study, constrain of soil on pipeline is simulated by soil springs. So soil spring parameters were used to investigate the influence of soil properties on pipe strain. For pipe deformation only occurs in vertical plane in this study, the influence of the lateral soil springs can be ignored. Thus, influences of the soil properties on the pipe strain was studied with respect to the following: the axial peak force per unit length (T_u), the vertical uplift peak force per unit length (Q_u), the vertical bearing peak force per unit length (Q_d), the yield displacement in the axial direction (Δt), the yield displacement for vertical uplift force (Δqu) and the yield displacement for vertical bearing force (Δqd).

According to the ALA Guideline (2001), the peak axial force per unit length of a pipe is

$$T_u = \pi D \alpha c + \pi D H \gamma \frac{1 + K_0}{2} \tan(f \phi) \quad (4)$$

with a yield displacement of

$$\begin{aligned} \Delta t &= 3\text{mm for dense sand} \\ &= 5\text{mm for loose sand} \\ &= 8\text{mm for stiff clay} \\ &= 10\text{mm for soft clay} \end{aligned} \quad (5)$$

where D is the pipe diameter, c is the soil cohesion representative, H is the depth of the soil from the ground surface to the center of the pipe, γ is the effective unit weight of the soil, K_0 is the coefficient of the lateral soil pressure at rest, and f is a reduction factor that depends on the outer-surface characteristics and the hardness of the pipe. ϕ is the internal friction angle of the soil. α is the adhesion factor, and $\alpha = 0.608 - 0.123c - \frac{0.274}{c^2 + 1} + \frac{0.695}{c^3 + 1}$.

The peak vertical uplift force per unit length of the pipe is

$$Q_u = N_{cv} c D + N_{qv} \gamma H D \quad (6)$$

with a yield displacement of

$$\begin{aligned} \Delta qu &= 0.01H \text{ to } 0.02H \text{ for dense to loose sand} \\ &= 0.1H \text{ to } 0.2H \text{ for stiff to soft sand} \end{aligned} \quad (7)$$

where N_{cv} is the vertical uplift factor for clay (0 for $c=0$) and N_{qv} is the vertical uplift factor for sand (0 for $\phi=0^\circ$). According to the ALA Guideline (2001), the parameters N_{cv} and N_{qv} are functions of the soil friction angle (ϕ) and the dimensionless pipe depth (H/D).

The peak vertical bearing force per unit length of the pipe is

$$Q_d = N_c c D + N_q \gamma H D + N_\gamma \gamma \frac{D^2}{2} \quad (8)$$

with a yield displacement of

$$\begin{aligned} \Delta qd &= 0.1D \text{ for granular soils} \\ &= 0.2D \text{ for cohesive soils} \end{aligned} \quad (9)$$

So the peak compressive strain of pipe can be assumed to be a function of all influence parameters as follows

$$\varepsilon = f(\delta_v, \psi, D, t, p, Q_u, Q_d, T_u, \Delta t, \Delta qu, \Delta qd) \quad (10)$$

Typical parameters of X80 steel pipeline in China were adopted in this study to conduct the parametric analysis. Especially large ranges of soil property parameters were considered to cover all possible cases in engineering application. It should be noticed that, when calculating the peak force and yield displacement of the axial soil spring, only the condition in which the pipeline is buried in the sandy soil was considered. Because, when the pipeline crosses an active fault with the native soil type of clay, the backfill soil should be replaced by sand to reduce the axial constrain of the pipeline (Q/SY GJX 0136, 2008). All soil property parameters were listed in Table 2. And for sand soil, soil cohesion representative c should set to be 0. Finally, based on the soil property values and Eqs. (4)-(9), the ranges of the peak forces per unit length and yield displacements in the axial and vertical directions can be derived, as shown in Table 3 with ranges of other three types of parameters.

The yield displacement of soil springs is relatively small comparing with the fault displacement applied on the pipe. Effects of the yield displacements of soil springs on the peak compressive strain is small. Therefore, reasonable independent dimensionless parameters were further selected to conduct the parametric analysis, which makes Eq. (10) transformed to Eq. (11)

$$\varepsilon = f\left(\frac{\delta_s}{L_a}, \frac{\psi}{180} \pi, \frac{D}{t}, \frac{p}{\sigma_0}, \frac{Q_u D^3}{EI}, \frac{Q_d D^3}{EI}, \frac{T_u D}{EA}\right) \quad (11)$$

where E is the initial elastic modulus; σ_0 is the yield stress of the pipe steel; I is the moment of inertia; A is the section area; L_a is unanchored pipe length, $L_a = \sigma_0 A / T_u$.

Consequently, the ranges of the dimensionless quantities can be derived, as listed in Table 4.

Table 2 Range of soil property values

Parameter type	Range of the values
Soil cohesion representative c (kPa)	0~80
Depth to pipe centerline H (m)	1.5~3.5
Effective unit weight of soil γ (kN/m ³)	14~28
Angle of friction ϕ (°)	20~40
reduction factor f	0.6~1

Table 3 Parameters range for X80 steel pipeline at reverse fault crossings

Parameter type	Parameters	Range of the parameter
Pipe parameters	Pipe diameter D (m)	1.016; 1.219; 1.422
	Pipe wall thickness t (m)	0.0184; 0.022; 0.0264; 0.033
	Internal pressure p (MPa)	0~12
Fault parameters	Fault displacement δ_v (m)	0~2.5
	Fault dip angle ψ (°)	0~90
Soil parameters	Peak axial force per unit length T_u (kN/m)	20~80
	Peak vertical uplift force per unit length Q_u (kN/m)	20~200
	Peak vertical bearing force per unit length Q_d (kN/m)	250~4500
	Axial yield displacement Δt (mm)	3~5
	Vertical uplift yield displacement Δqu (mm)	15~350
	Vertical bearing yield displacement Δqd (mm)	102~284

Table 4 Ranges of the dimensionless parameters

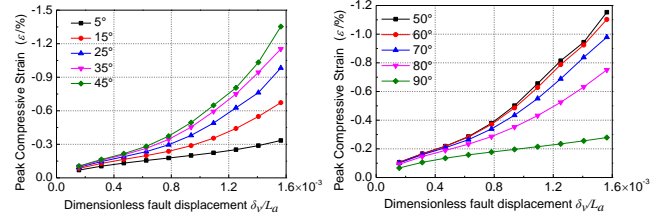
Dimensionless Parameters	Ranges
δ_s/L_a	0~ 2×10^{-3}
$\psi\pi/180$	0~ 0.5π
D/t	37~66
p/σ_0	0~0.0226
$T_u D/(EA)$	1.43×10^{-6} ~ 7.15×10^{-6}
$Q_u D^3/(EI)$	0.9×10^{-5} ~ 9×10^{-5}
$Q_d D^3/(EI)$	1.22×10^{-4} ~ 19.48×10^{-4}

Parametric analysis was conducted to elucidate the relationship between the strain demand and the dimensionless parameters listed above.

2340 cases with different combinations of parameters were considered. The main reason is that because effects of the soil spring parameters on pipe strain are more complicated for reverse fault than the ones for strike-slip fault. Large number of cases are needed to investigate the relationship of soil parameters and the strain as well as the influence among these parameters, and details will be discussed in the following parts.

4.2 Effects of the fault displacement and dip angle on strain demand

When a pipeline is subjected to reverse fault displacement, it undergoes combined compression and bending induced by fault displacement (δ_v) and dip angle (ψ), which is similar to the stress state for pipeline subjected to a compression strike-slip fault movement (Xie 2008, Liu *et al.* 2016). And if ψ is close to 0°, the compression effect is more prevailing. If the dip angle ψ is close to 90°, the bending effect is more prevailing. If ψ is close to 45° the combining effect is most severe.



(a) Fault dip angle (ψ) between 0° and 45° (b) Fault dip angle (ψ) between 45° and 90°

Fig. 8 Relationship between the strain demand (ε) and the fault displacement (δ_s) at different fault dip angles

Trends of the strain demand (ε) with the dimensionless fault displacement (δ_v/L_a) at different fault dip angles were discussed here, and totally 270 cases were considered. The baseline parameters are as follows: pipe diameter $D=1.219$ m, pipe wall thickness $t=0.022$ m, and internal pressure $p=12$ MPa. The pipe was assumed to be buried in a medium sand, of which the peak vertical uplift force per unit length Q_u is 50 kN/m with a yield displacement $\Delta qu=1.5$ mm, the peak vertical bearing force per unit length Q_d is 2000 kN/m with yield displacement $\Delta qd=121.9$ mm, and the peak axial force per unit length T_u is 45 kN/m, with axial yield displacement $\Delta t=3$ mm.

As shown in Fig. 8, ε increases with the increase of δ_v/L_a . And it increases faster for large value of δ_v/L_a , which is consistent with the relationship of ε with fault displacement at compression strike-slip fault (Liu *et al.* 2016). Fig. 8(a) illustrated that, if dip angle is less than 45° ($\psi\pi/180 < 0.25\pi$), ε increases as $\psi\pi/180$ increases. Fig. 8(b) illustrated that, if dip angle is between 45° and 60° ($0.25\pi < \psi\pi/180 < 0.66\pi$), ε decreases a little as $\psi\pi/180$ increases; while if dip angle is larger than 60° ($\psi\pi/180 > 0.66\pi$), ε decreases as $\psi\pi/180$ increases. Thus the peak pipe axial compressive strain peaks when the dip angle is between 45° and 50°. Similar results can also be obtained for conditions with other soil and internal pressure parameters.

4.3 Effects of pipe diameter and wall thickness on strain demand

The pipe diameter (D) and wall thickness (t) have a direct effect on pipe axial and bending stiffness, which will eventually have a significant effect on the pipe compressive strain. In service conditions, axial strain induced by internal pressure of the pipe is also effected by ratio of D/t . So trends of ε with D/t in various conditions were investigated in detail here.

Soil parameters as well as internal pressure adopted in Section 4.2 are also used here. Three dip angles, i.e., 30°, 45°, 60°, were considered. Results from 180 cases show that, trends of ε with D/t are similar for different dip angles. Thus, typical results for dip angle of 45° were elaborated. Fig. 9 illustrates the peak compressive strain with various ratios of diameter to wall thicknesses (D/t) with different diameters when the fault displacement is 0.6 m ($\delta_v/L_a=4.69 \times 10^{-4}$). It can be derived that, for a constant diameter, ε increases with D/t increase. It should be also noticed that, for the same value of D/t , ε decreases with D

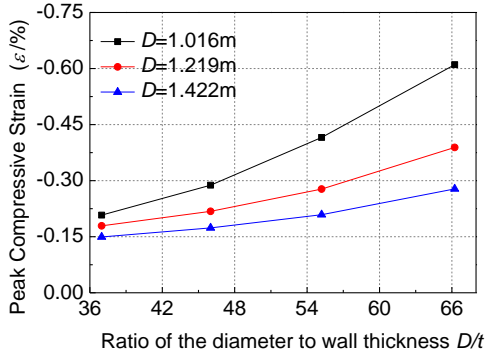


Fig. 9 Relationship between the strain demand (ε) and the ratio of the diameter to wall thickness (D/t) with different pipe diameters

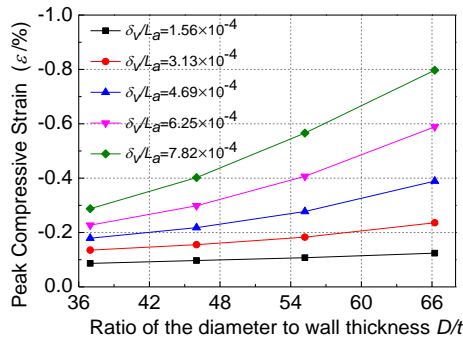


Fig. 10 Relationship between the strain demand (ε) and the ratio of the diameter to wall thickness (D/t) under different fault displacements

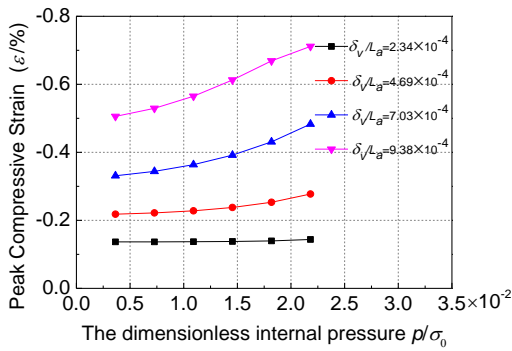


Fig. 11 Relationship between the strain demand (ε) and the dimensionless internal pressure (p/σ_0) at different fault displacements

increases. Fig. 10 illustrates the peak compressive strain with various ratio of diameters to wall thicknesses (D/t) under different fault displacements when the pipe diameter was set to 1.219 m. Trends of ε with D/t are similar for all fault displacements, and ε increases more sharply at a larger fault displacement.

4.4 Effects of internal pressure on strain demand

Internal pressure is a main service load for pipe structures. When the pipe is under compression, internal pressure increases the axial compressive strain due to

Poisson effect (Liu *et al.* 2016). The maximum internal pressure P_{max} is set to 12 MPa according to ASME B31.8 (2007). Six internal pressure values were considered to investigate the relationship between the strain demand ε and internal pressure quantitatively. The same baseline parameters for soil and fault parameters adopted in Section 4.3 are used here. The pipe with diameter of 1.219 m and wall thickness of 0.022 m is considered. Totally 90 cases are investigated. As shown in Fig. 11, ε increases as p/σ_0 increases. And trends are similar for all fault displacements, but a larger fault displacement will lead to a larger peak compressive strain.

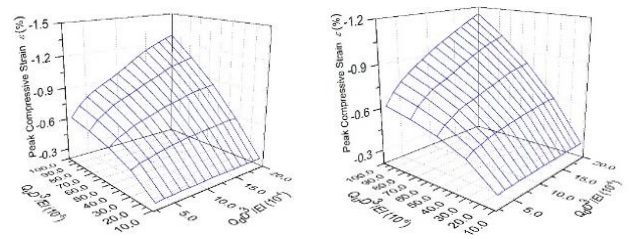
4.5 Effects of soil properties on strain demand

The main influences on pipe strain caused by soil properties can be represented by the peak soil forces, for effects caused by the yield displacements of soil springs are very small (Liu *et al.* 2016). The peak axial force per unit length T_u results in pipe axial strain, while the peak vertical uplift and bearing force Q_u, Q_d result in pipe bending strain.

In this section, pipe parameters used in Section 4.2 are adopted. The internal pressure was set to 12 MPa. Three dip angles, i.e., 30°, 45°, 60°, as well as five fault displacements ranging from 0.2 m to 1m were considered to derive strain results. To investigate the influences of three soil peak forces, possible combinations for them are all considered for each fault displacement and dip angle, which makes the total number of considered cases in this section up to 1800. Results show that, similar trends occur between the strain demand and the soil peak forces, and the relationships between these three peak soil forces and the pipe strain can be considered as independent. Thus only typical results were discussed below.

Fig. 12 illustrates the effects of the dimensionless peak vertical uplift and bearing force per unit length ($Q_u D^3/(EI)$ and $Q_d D^3/(EI)$) on the peak compressive strain ε . Results show that ε increases as $Q_u D^3/(EI)$ and $Q_d D^3/(EI)$ increase. By comparing Fig. 12(a) and Fig. 12(b), this trend remains the same for cases with different peak axial force per unit length and fault displacement.

Detailed relationship between the strain demand ε and the peak axial force per unit length T_u was also studied as shown in Fig. 13. ε increases as $T_u D/(EA)$ increases. And the regularity of this relationship is similar for different peak vertical bearing forces.



(a) Fault displacement $\delta_v = 1$ m, peak axial force per unit length $T_u = 20$ kN/m
 (b) Fault displacement $\delta_v = 0.8$ m, peak axial force per unit length $T_u = 40$ kN/m

Fig. 12 Trends of ε with $Q_u D^3/(EI)$ and $Q_d D^3/(EI)$

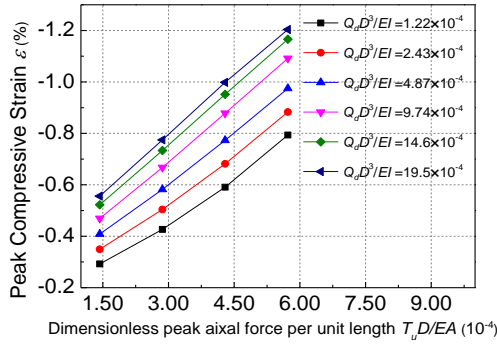


Fig. 13 Relationship between the strain demand (ε) and the peak axial force per unit length ($T_u D/(EA)$)

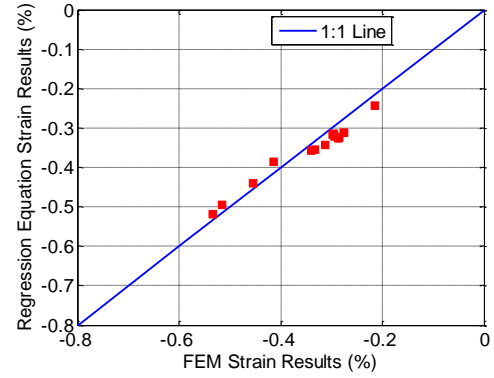


Fig. 14 Comparison of the predicted results and the numerical results for reverse fault in vertical plane

5. Regression equation for strain demand of X80 pipe crossing reverse fault

5.1 Regression equation

The main purpose of this study is to propose a regression based prediction model for strain demand of X80 pipe at reverse fault crossings. Thus, 2340 numerical strain results for different combinations of all parameters were analyzed in Section 4. And their functional relationships with strain demand can be assumed to form the assumed equation (Eq. (12)). Mostly, power functions are used. And some coupling effects were considered by changing the exponent of power function with related parameters

$$\varepsilon = a_1 \left(\frac{\delta_s}{L_a} \right)^{\left(-(\pi\psi/180-1/4\pi)^2 + a_2\pi\psi/180 + a_3 + a_4 \left(\frac{p}{\sigma_s} \right) \right)} \left(\frac{D}{t} \right)^{a_5} \left(\left(\frac{p}{\sigma_s} \right) + a_7 \right) \left((\pi\psi/180-1/4\pi)^2 + a_8 \right) \left(\frac{Q_u D^3}{EI} \right)^{a_9} \left(\frac{Q_d D^3}{EI} \right)^{a_{10}} \left(\frac{T_u D}{EA} \right)^{a_{11}} + a_{12} \quad (12)$$

where D is the pipe diameter (m), t is the pipe wall thickness (m), δ_s is the fault displacement (m), ψ is the fault dip angle ($^\circ$), σ_0 is the yield stress (MPa), p is the internal pressure (Pa), T_u is the peak axial force per unit length (KN/m), Q_u and Q_d are the peak vertical uplift and bearing force per unit length (KN/m), I is the moment of inertia (m^4); A is the section area (m^2); L_a is unanchored pipe length (km), and $a_1 \sim a_{12}$ are nonlinear regression coefficients, which are determined as

$$\begin{aligned} a_1 &= -2.9596 \times 10^{-4} & a_7 &= 1.465 \times 10^{-3} \\ a_2 &= -0.2015 & a_8 &= -0.7634 \\ a_3 &= 2.1260 & a_9 &= 0.5058 \\ a_4 &= -26.14 & a_{10} &= 0.1821 \\ a_5 &= 1.295 & a_{11} &= -0.7768 \\ a_6 &= 9.013 & a_{12} &= -4.9095 \times 10^{-4} \end{aligned} \quad (13)$$

It should be noticed that the pipe-fault crossing angle was not included in this equation. But effects of pipe-fault crossing angle on pipe strain can be considered according Section 6.1.

5.2 Equation validation

15 design cases in the Second West to East Gas Pipeline were examined here to validate the accuracy of the proposed equation. Fault parameters for all cases are listed in Table 6. For the proposed equation is limited for pipeline displacement in the vertical plane, only the vertical and axial displacements of all cases were considered in this section. Fig. 14 illustrates the comparison results of the proposed model and numerical results calculated by finite element models. It can be derived that the predicted strain result of the proposed model is accurate.

6. Application to oblique-reverse faults

6.1 Strain demand estimation procedure for X80 steel pipeline crossing oblique-reverse faults

As mentioned in the Introduction part, active faults attempted by buried pipelines in practice are generally oblique-reverse fault composed of both reverse fault and strike-slip fault. Under this circumstance, the pipeline deforms spatially. Karamitros *et al.* (2011) found that, for (oblique) normal fault, the pipeline deformation in the horizontal and vertical plane is not superimposed, because the different values of soil resistance in the vertical and horizontal plane lead to the maximum bending moments and longitudinal strains occur at different points along the pipeline axis. Our numerous results indicate that this phenomenon is also suitable for oblique-reverse faulting. The reason is that usually the maximum bending strain caused by vertical displacements is at pipe invert and near the fault trace, while the maximum bending strain caused by horizontal displacements is at the lateral side and farther way from the fault trace. Thus, a general 3D case for oblique-reverse fault can be approximately decomposed into two simpler 2D cases with the same fault displacements in horizontal or vertical plane. Based on this, using the proposed model and the previous one for compression strike-slip fault (Liu *et al.* 2016), it is possible to obtain the peak compressive strain for pipelines crossing common oblique-reverse faults. The main procedure is

elucidated as follows:

Firstly, fault displacements in axial, lateral and vertical directions of the pipeline axis can be obtained easily by algebraically addition of the strike-slip displacement components and reverse displacement components by Eq. (14). The geometrical sketch of buried pipeline crossing oblique-reverse fault is shown in Fig. 15

$$\begin{cases} \Delta X = \delta_v \cos \varphi \sin \beta + \delta_s \cos \beta \\ \Delta Z = -\delta_v \cos \varphi \cos \beta + \delta_s \sin \beta \\ \Delta Y = -\delta_v \sin \varphi \end{cases} \quad (14)$$

The horizontal part can be converted to a compression strike-slip fault with axial displacement of ΔX and lateral displacement of ΔZ . The equivalent fault displacement δ_{sequal} and equivalent strike-slip fault crossing angle β_{equal} can be calculated as follows

$$\begin{cases} \delta_{sequal} = \sqrt{\Delta X^2 + \Delta Z^2} \\ \beta_{equal} = \arctan(\Delta Z / \Delta X) \end{cases} \quad (15)$$

On the basis of the derived equivalent strike-slip fault parameters, the peak compressive strain in the horizontal plane ε_{sequal} can be obtained by the strain prediction model of Liu *et al.* (2016) suitable for compression strike-slip fault.

The vertical part can be converted to a reverse fault in vertical plane with axial displacement of ΔX and vertical displacement of ΔY . The equivalent fault displacement δ_{vequal} and equivalent reverse fault dip angle ψ_{equal} can be calculated as follows

$$\begin{cases} \delta_{vequal} = \sqrt{\Delta X^2 + \Delta Y^2} \\ \varphi_{equal} = \arctan(\Delta Y / \Delta X) \end{cases} \quad (16)$$

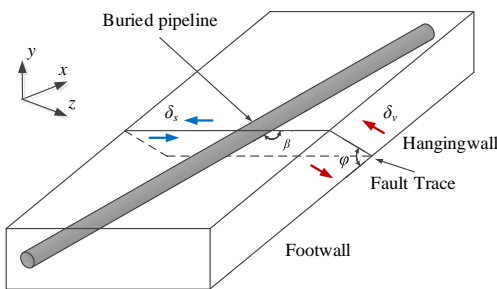


Fig. 15 Schematic representation of buried pipeline crossing oblique-reverse faults

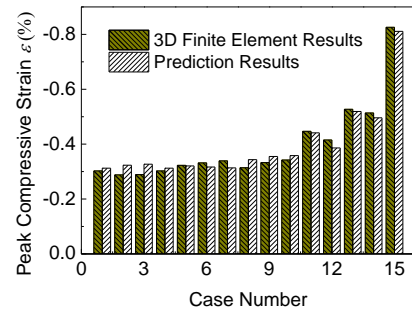
On the basis of the derived equivalent reverse fault parameters, the peak compressive strain in the vertical plane ε_{vequal} can be obtained by the strain prediction equation in Section 5.1 (Eq. (12)).

Finally, the strain demand $\varepsilon_{oblique}$ for pipeline at oblique-reverse fault crossing can be obtained by taking the maximum strain in absolute values of the two parts:

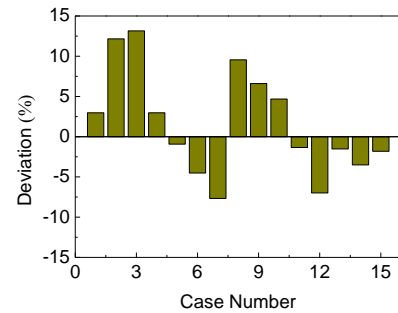
$$\varepsilon_{oblique} = \max(\varepsilon_{sequal}, \varepsilon_{vequal})$$

6.2 Cases study for the Second West to East Gas pipeline

In order to check the accuracy of the proposed strain estimation method, 15 real cases for four active faults faced by the West to East Gas pipeline are considered. All the faults are located in the Gobi Desert in the northwest of China. According to Q/SY GJX 0136, 2008, the soil types were considered as dense sand soils. The pipe diameter and pipe wall thickness were 1.219 m and 0.022 m, respectively. The maximum operating pressure of the pipe was 12 MPa.



(a) 3D FEM results and the regression equation results for all cases



(b) Deviation between the 3D FEM results and the regression equation results

Fig. 16 Comparison of the proposed method and 3D nonlinear finite element model

Table 5 Detailed soil parameters for the active faults

Active Fault Name	Effective unit weight of soil γ (kN/m ³)	Angle of friction ϕ (°)	Soil cohesion representative c (kPa)	Axial force per unit length T_u (kN/m)	Lateral peak force per unit length P_u (kN/m)	Vertical uplift force per unit length Q_u (kN/m)	Vertical bearing force per unit length Q_d (kN/m)
Xishan Fault	22	33	0	39	395	53	1769
Wangjiagou Fault	19	34	0	35	368	47	1754
Yinwashedan Fault	20	34	0	36	388	50	1846
Tianqiaogou Fault	16	36	0	30	362	42	1961

Table 6 Parameters for 15 real design cases in the Second West to East Gas Pipeline Project

Active Fault Name	Case number	Strike-slip fault displacement δ_s (m)	Reverse fault displacement δ_r (m)	Possible crossing angle β (°)	Possible dip angle ψ (°)	Axial displacement ΔX (m)	Lateral displacement ΔZ (m)	Vertical displacement ΔY (m)
Xishan Fault	1	0.5	-0.5	120	40	-0.58	0.24	0.32
	2	0.5	-0.5	130	40	-0.61	0.13	0.32
	3	0.5	-0.5	136	40	-0.62	0.07	0.32
Wangjiagou Fault	4	0.5	-0.5	120	50	-0.53	0.27	0.38
	5	0.5	-0.5	120	60	-0.46	0.30	0.43
	6	0.5	-0.5	120	70	-0.40	0.34	0.47
	7	0.5	-0.5	150	50	-0.59	-0.03	0.38
	8	0.5	-0.5	150	60	-0.56	0.03	0.43
	9	0.5	-0.5	150	70	-0.51	0.10	0.47
Yinwashan Fault	10	0	-1	139	60	-0.33	-0.38	0.87
	11	0	-1	139	70	-0.22	-0.26	0.94
	12	0	-1	120	50	-0.56	-0.32	0.77
	13	0	-1	120	60	-0.43	-0.25	0.87
	14	0	-1	120	70	-0.30	-0.17	0.94
Tianqiaogou Fault	15	1.31	-0.5	90	70	-0.17	1.31	0.47

Buried depth of pipe is 1.8 m. Pipe coating was fusion bonded epoxy. The backfill soils were same as the native soil. The detailed soil parameters suggested by Q/SY GJX 0136, 2008 for the four faults are listed below in Table 5.

Fault displacement components were also calculated according to Eq. (14), as listed in Table 6. On the basis of all these parameters, the peak compressive strain for equalized compressive strike-slip fault and reverse fault in vertical plane were calculated according to the procedure described in Section 6.1. Finally the peak compressive strain $\varepsilon_{oblique}$ is obtained. A 3D nonlinear finite element model was also performed to validate the predicted strain results. Fig. 16 illustrates the comparison results. It can be derived that, the maximum deviation is only 13%. From an engineering point of view, this proposed method can provide rather good prediction results.

7. Conclusions

A strain demand calculation procedure of buried X80 steel pipeline crossing (oblique) reverse faults was proposed in this study. An improved numerical model was adopted and validated by the latest full scale experimental data. Effects of all influence factors on strain demand were systematically investigated, especially the soil parameters. Quantitative relationships of the strain demand and all the affecting factors were obtained. Based on parametric analysis results, a regression equation was proposed and validated. Finally, a strain demand estimation method for X80 pipeline crossing 3D oblique-reverse faulting was presented by combining the proposed semi empirical model for reverse fault and the previous one for compression strike-slip fault (Liu *et al.* 2016). By comparing with 3D nonlinear finite element results for fifteen real design cases

faced by the Second West to East Gas Pipeline, this method was proven to be able to provide accurate strain predictions. The proposed method can be directly used for strain demand calculation for X80 steel pipelines in seismic areas in engineering practice for it saves much time and computational power consumption and results are also reliable as the FE model.

Acknowledgments

The research described in this paper was financially supported by CNPC Fund for Science and Technology Special Project under Grant No. 2012E-2801, National Key Research and Development Program under Grant No. 2016YFC0802105, Opening fund of State Key Laboratory of Coastal and Offshore Engineering (Dalian University of Technology) under Grant No. LP1507, Opening fund of State Key Laboratory of Ocean Engineering (Shanghai Jiao Tong University) under Grant No 1314, Opening fund of State Key Laboratory of Hydraulic Engineering Simulation and Safety (Tianjin University) under Grant No HESS-1411 and Science Foundation of China University of Petroleum, Beijing under Grant No. 2462015YQ0408, No. C201602 and No. 2462015YQ0403.

References

- ABAQUS (2011), ABAQUS user's manual, version 6.11, Simulia, USA.
- American Lifelines Alliance-ASCE (2001), *Guidelines for the design of buried steel pipe*. ASCE, USA.
- American Society of Mechanical Engineers, B31.8 (2007), *Gas transmission and distribution piping systems*. ASME, USA.
- Canadian Standards Association, Z662 (2007), *Oil and gas*

- pipeline systems. CSA, Canada.
- European Committee For Standardization, EN 1998 (1998), *Design of structures for earthquake resistance. Part 4. Silos, tanks and pipelines*.
- Gantes, C.J. and Bouckovalas, G.D. (2013), "Seismic verification of the high pressure natural gas pipeline Komotini-Alexandroupolis-Kipi in areas of active fault crossings", *Struct. Eng. Int.*, **23**(2), 204-208.
- Gu, X. and Zhang, H. (2009), "Research on aseismatic measures of gas pipeline crossing a fault for strain-based design", *ASME 2009 Pressure Vessels and Piping Conference*, 571-580.
- Ha, D. (2007), "Evaluation of ground rupture effect on buried HDPE pipelines", Department of Civil and Environmental Engineering, Rensselaer Polytechnic Institute.
- Jalali, H.H., Rofooei, F.R., Attari, N.K.A. and Samadian, M. (2016), "Experimental and finite element study of the reverse faulting effects on buried continuous steel gas pipelines", *Soil Dyn. Earthq. Eng.*, **86**, 1-14.
- Joshi, S., Prashant, A., Deb, A. and Jain, S.K. (2011), "Analysis of buried pipelines subjected to reverse fault motion", *Soil Dyn. Earthq. Eng.*, **31**(7), 930-940.
- Karamitros, D.K., Bouckovalas, G.D. and Kouretzis, G.P. (2007), "Stress analysis of buried steel pipelines at strike-slip fault crossings", *Soil Dyn. Earthq. Eng.*, **27**(3), 200-211.
- Karamitros, D.K., Bouckovalas, G.D., Kouretzis, G.P. and Gkesouli, V. (2011), "An analytical method for strength verification of buried steel pipelines at normal fault crossings", *Soil Dyn. Earthq. Eng.*, **31**(11), 1452-1464.
- Karamitros, D.K., Zoupantis, Ch. and Bouckovalas, G.D. (2016), "Buried pipelines with bends: analytical verification against permanent ground displacements", *Can. Geotech. J.*, **53**(11), 1782-1793.
- Kennedy, R.P., Chow, A.M. and Williamson, R.A. (1977), "Fault movement effects on buried oil pipeline", *Transp. Eng. J. Am. Soc. Civ. Eng.*, **103**(6), 617-633.
- Liu, A., Hu, Y., Zhao, F., Li, X., Takada, S. and Zhao, L. (2004), "An equivalent-boundary method for the shell analysis of buried pipelines under fault movement", *Acta Seismol. Sin.* **17**(s1), 150-156.
- Liu, B., Liu, X.L. and Zhang, H. (2009), "strain-based design criteria of pipelines", *J. Loss Prevent. Proc.*, **22**(6), 884-888.
- Liu, M., Wang, Y.Y. and Yu, Z. (2008), "Response of pipelines under fault crossing", *Proceedings of the Eighteenth(2008) International Offshore and Polar Engineering Conference*, 162-165.
- Liu, X.B., Zhang, H. and Chen, Y.F. (2015), "Strain prediction of X80 steel pipeline at strike-slip fault under compression combined with bending", *ASME 2015 Pressure Vessels & Piping Conference*, Boston, USA.
- Liu, X.B., Zhang, H., Han, Y.S., Xia, M.Y. and Zheng, W. (2016), "A semi-empirical model for peak strain prediction of buried X80 steel pipelines under compression and bending at strike-slip fault crossings", *J. Nat. Gas Sci. Eng.*, **32**, 465-475.
- Liu, X.B., Zhang, H., Li, M., Xia, M.Y., Zheng, W., Wu, K. and Han, Y.S. (2016), "Effects of steel properties on the local buckling response of high strength pipelines subjected to reverse faulting", *J. Nat. Gas Sci. Eng.*, **33**, 378-387.
- Lower, Mark D. (2014), "Strain-based design methodology of large diameter grade X80 linepipe", Ph.D. dissertation, University of Tennessee.
- Melissianos, V.E., Korakitis, G.P., Gantes, C.J. and Bouckovalas, G.D. (2016), "Numerical evaluation of the effectiveness of flexible joints in buried pipelines subjected to strike-slip fault rupture", *Soil Dyn. Earthq. Eng.*, **90**, 395-410.
- Melissianos, V.E. and Gantes, C.J. (2016), "Numerical modeling aspects of buried pipeline - fault crossing", *Comput. Methods Earthq. Eng.*, **3**, 1-26.
- Mohr, W. (2003), "Strain-based design of pipelines - Project No. 45892GTH", Columbus, USA.
- Newmark, N.M. and Hall, W.J. (1975), "Pipeline design to resist large fault displacement", *The US National Conference on Earthquake Engineering*.
- O'Rourke, M.J. and Liu, X. (2012), "Seismic design of buried and offshore pipelines", Multidisciplinary Center for Earthquake Engineering Research, University at Buffalo.
- Q/SY GJX 0136 (2008), *Guideline for strain-based design in seismic area and active fault crossing of the second west-east natural gas transportation pipeline project*, PetroChina Co Ltd, China.
- Ramberg, W. and Osgood, W.R. (1943), "Description of stress-strain curves by three parameters", Technical Report Archive & Image Library, USA.
- Rofooei, F.R., Hojat Jalali, H., Attari Nader, K.A. and Alavi, M. (2012), "Full-scale laboratory testing of buried pipelines subjected to permanent ground displacement caused by reverse faulting", *Proceedings of the 15th World Conference on Earthquake Engineering*, Lisboa, Portugal, September.
- Rofooei, F.R., Jalali, H.H., Attari, N.K.A. and Samadian, M. (2015), "Parametric study of buried steel and high density polyethylene gas pipelines due to oblique-reverse faulting", *Can. J. Civ. Eng.*, **42**(3), 178-189.
- Saberi, M., Behnamfar, F. and Vafaeian, M. (2013), "A semi-analytical model for estimating seismic behavior of buried steel pipes at bend point under propagating waves", *Bull. Earthq. Eng.*, **11**(5), 1373-1402.
- Shokouhi, S.K.S., Dolatshah, A. and Ghobakhloo, E. (2013), "Seismic strain analysis of buried pipelines in a fault zone using hybrid FEM-ANN approach", *Earthq. Struct.*, **5**(4), 417-438.
- Takada, S., Hassani, N. and Fukuda, K. (2001), "A new proposal for simplified design of buried steel pipes crossing active faults", *Earthq. Eng. Struct. Dyn.*, **30**(8), 1243-1257.
- Trifonov, O.V. (2014), "Numerical stress-strain analysis of buried steel pipelines crossing active strike-slip faults with an emphasis on fault modeling aspects", *J. Pipeline Syst. Eng. Pract.*, **6**(1), 4014008.
- Trifonov, O.V. and Cherniy, V.P. (2010), "A semi-analytical approach to a nonlinear stress-strain analysis of buried steel pipelines crossing active faults", *Soil Dyn. Earthq. Eng.*, **30**(11), 1298-1308.
- Trifonov, O.V. and Cherniy, V.P. (2012), "Elastoplastic stress-strain analysis of buried steel pipelines subjected to fault displacements with account for service loads", *Soil Dyn. Earthq. Eng.*, **33**(1), 54-62.
- Uckan, E.B., Anbas, J.S., Wou, R., Paolacci, F. and O'Rourke, M.J. (2015), "A simplified analysis model for determining the seismic response of buried steel pipes at strike-slip fault crossings", *Soil Dyn. Earthq. Eng.*, **75**, 55-65.
- Vazouras, P., Karamanos, S.A. and Dakoulas, P. (2010), "Finite element analysis of buried steel pipelines under strike-slip fault displacements", *Soil Dyn. Earthq. Eng.*, **30**(11), 1361-1376.
- Vazouras, P., Karamanos, S.A. and Dakoulas, P. (2012), "Mechanical behavior of buried steel pipes crossing active strike-slip faults", *Soil Dyn. Earthq. Eng.*, **41**(5), 164-180.
- Vazouras, P., Dakoulas, P. and Karamanos, S.A. (2015), "Pipe-soil interaction and pipeline performance under strike-slip fault movements", *Soil Dyn. Earthq. Eng.*, **72**(4), 48-65.
- Wang, L.R.L. and Yeh, Y.H. (1985), "A refined seismic analysis and design of buried pipeline for fault movement", *Earthq. Eng. Struct. Dyn.*, **13**(1), 75-96.
- Xie, X.J. (2008), "Numerical analysis and evaluation of buried pipeline response to earthquake-induced ground fault rupture", Ph.D. dissertation Department of Civil and Environmental Engineering, Rensselaer Polytechnic Institute.
- Zhang, J., Liang, Z. and Han, C.J. (2014), "Buckling behavior

analysis of buried gas pipeline under strike-slip fault displacement”, *J. Nat. Gas Sci. Eng.*, **21**, 921-928.

Zheng, W., Zhang, H., Liu, X.B., Liang, L.C. and Han, Y.S. (2016), “Contrastive study on finite element models of high-strength pipelines crossing active faults”, *Mater. Sci. Forum*, **850**, 957-964.

AT